Dual-direction Measuring System of Near Infrared Optical Tomography Combined with X-ray Mammography

Hung-Chih Chiang[1]
Jhao-Ming Yu[1]
Liang-Yu Chen[1]
Min-Chun Pan[1]

1. Department of Mechanical Engineering, National Central University

Min-Cheng Pan[2,*]
Ching-Tang Wu[3]

2. Department of Electronic Engineering, Tung-Nan University
*Corresponding author e-mail: m2pan@mail.tnu.edu.tw
3. Tao-Yuan General Hospital, DOH, Taiwan

Abstract

This study is to develop a dual-direction measuring instrument of diffuse optical tomography in the continue-wave domain to be incorporated with an X-ray mammography system for the aid of obtaining functional images to detect breast tumors. The device is handled to compress breast-like phantoms by two slabs with sources and detectors which a multiple-channel switching was designed for. Obtained from a dual-direction projection, collaborative information can be benefit for image reconstruction as compared with a single-direction information used. Finally, both simulation data and experimental data are performed to reconstruct functional optical-coefficient images.

1. Introduction

The most common used non-invasive biomedical imaging modality of breast diagnosis, such as sonography and X-ray mammography, can acquire structural information of breast tissue. However, those imaging modalities are still trapped in overlapping structures, resulting in false diagnosis; moreover, X-ray mammography involves ionizing radioactivity. Diffuse optical tomography (DOT) is an emerging technique which can provide physiological or pathological information about the breast. On the other hand, DOT is inexpensive and non-ionizing [1]. Since NIR laser light passes through the tested phantom or tissue, optical variations responsive to tissue, power attenuation and phase difference, can be measured. Subsequently, both the absorption and scattering distribution of the breast can be obtained with using image reconstruction algorithm. Further, utilizing optical properties is capable of evaluating oxyhemoglobin, deoxyhemoglobin, water, and lipid concentration in the breast. This paper is organized as follows. Section 2 describes the instrumentation of dual-direction scanning device. Then, the image reconstruction algorithm is presented in Sec 3. Section 4 shows some results were achieved from the application of instrumentation and computation where a likely area was used in some cases. Finally, concluding remark is made in Sec. 5.

2. Instrumentation: Dual-direction Scanning Device

The NIR DOT scanning device is set up on a special plate compatible with the apparatus of X-ray mammography; therefore, the device is handled by compressing breast with two slabs to shorten the distance between sources and detectors capable of enhancing SNR during a measuring process as in previous researches the slab-type scanning device was designed for this advantage [2][3]. In previous designs, however, the reconstruction image quality is restricted to available data obtained from single-direction information. Compared with a single-direction projection used as usual, the dual-direction projection scanning device is designed as two pairs of dual 1-D scanning array of 7 by 7 source-and-detector combination separately distributed on the upper and lower slabs where one is for acquiring data from the bottom and the other is from the top shown as Fig. 1. By means of this measuring device, more information can be acquired to obtain a better optical-property image quality.

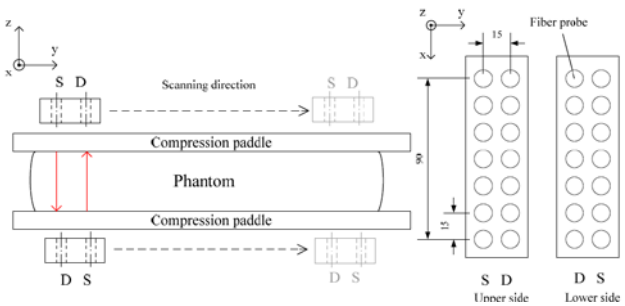

Figure 1. Diagram of dual-direction projection scanning device.

2.1 Architecture of measuring system

Dual-direction projection scanning device is consisted of four major parts including (1) source part, (2) mechanical part, (3) detector part, and (4) signal processing part as

shown in Fig. 2. In source and detector parts, our design

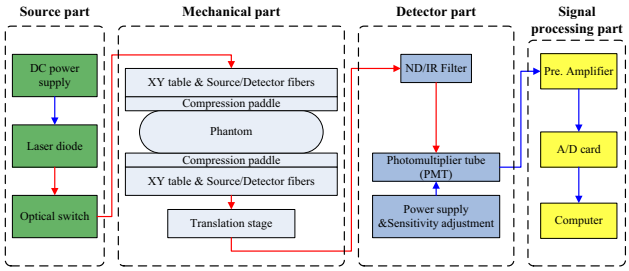

Figure 2. Architecture of continuous-wave measuring system.

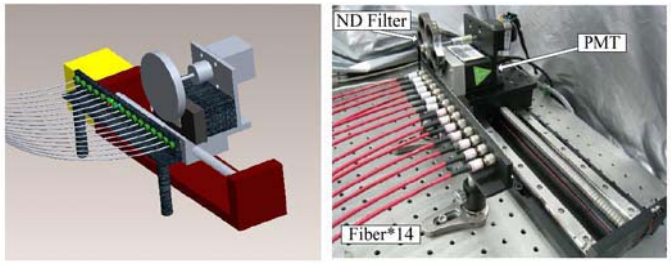

Figure 3. (a) Prototype design and (b) photograph of translation stage.

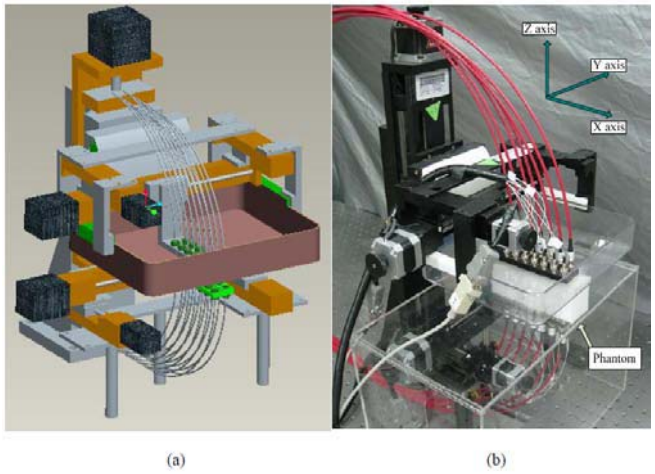

Figure 4. (a) Prototype design and (b) photograph of mechanical part.

provides multi-channel with faster source/detector switching speed (Fig. 3). As can be seen, the sources and detectors are installed on the 3D translation stage, of which movement can be controllable with a computer. Mechanical part also provides measurement adaptability to a compressible phantom/tissue with the help of XY slabs and controllable source/detector array (Fig. 4.).

2.1 Measuring mechanism

This measuring system is operated in the continuous wave domain shown as Fig. 2 [4]. First of all, DC power supply provides laser diode with a static voltage that leads to output a constant NIR light power. Subsequently, NIR light is transmitted to each source position on source array by an optical switch. Then, the source light passes through the tested phantom and the diffuse light emitted from the phantom at each detector (PMT) is acquired with seven separable fibers; prior to detectors, the diffuse light passes though an adaptive neutral density filter and an IR filter in order to attenuate optical power and filter out other wavelength, respectively. Finally, a photomultiplier tubes (PMT) transforms optical intensity into electric current. In signal processing part, the output current is converted into voltage and amplified about 40dB with a preamplifier. The amplified voltage signal is acquired and recorded with a data acquisition device.

3. Image Reconstruction Algorithm

The image reconstruction algorithm of DOT based on the diffusion equation involves both the computation of a forward problem and the regularization of an inverse problem. The continue wave diffusion equation (Eq. (1)) is used to describe light transporting in a highly scattering medium such as breast tissue [5].

$$\nabla \cdot D\nabla\Phi(r) - \mu_a\Phi(r) = -S_o(r), \qquad (1)$$

where Φ is intensity, μ_a is the absorption coefficient in mm^{-1} and D is the diffusion coefficient in mm.

3.1 Forward computation

The forward computation uses a finite element method (FEM) for solving diffusion equation to estimate the distribution of transmitted light on the basis of the light source and presumed parameters of the phantom. Type III or Robbins boundary conditions are used at all boundary nodes, where the exiting flux ($J \cdot \hat{n}$) (Eq. (2)) normal to the boundary is proportional to the fluency rate (F) at the boundary [6],

$$J \cdot \hat{n} = F = -D\nabla\Phi \cdot \hat{n} = \alpha\Phi, \qquad (2)$$

where $\hat{n}$ is the unit vector normal to the boundary and α is a real positive number relating to the internal reflection. Meantime, the Galerkin method is applied in FEM to Eq. (1) and the following discrete equation can be obtained.

$$\begin{bmatrix} A_{ij}^{bb} - \alpha B_{ij}^{bb} & A_{ij}^{bI} \\ A_{ij}^{Ib} & A_{ij}^{II} \end{bmatrix} \begin{Bmatrix} \Phi_j^b \\ \Phi_j^I \end{Bmatrix} = \begin{Bmatrix} C_i^b \\ C_i^I \end{Bmatrix} \qquad (3)$$

3.2 Inverse reconstruction

The image reconstruction procedure is a nonlinear, ill-posed, and ill-determined problem. In absence of an analytic inverse solution, the numerical way of achieving this inverse solution is to minimize the difference between measured intensity and forward computation intensity; i.e. ,

$$\min \sum_{i=1}^{N} \left[\Phi_i^M - \Phi_i^C \right]^2, \qquad (4)$$

where Φ_i^M and Φ_i^C are measured and computation intensity, respectively. The Levenberg-Marquardt algorithm is adopted for iteratively updating the diffusion and absorption coefficients [7], i.e.

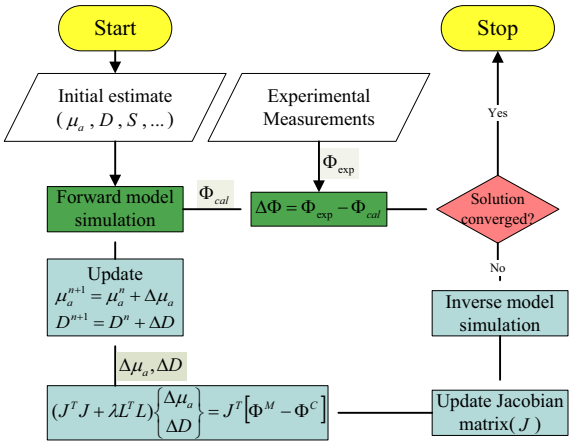

Figure 5. Flowchart of optical-property image reconstruction algorithm.

$$\begin{bmatrix}\Delta\mu_a \\ \Delta D\end{bmatrix} = \left([J]^T[J] + \lambda I\right)^{-1}[J]^T\left[\Phi^M - \Phi^C\right], \quad (5)$$

Where $[J]$ (Jacobian matrix) is an optical-property matrix that denotes $J(\frac{\partial\Phi_b}{\partial D}, \frac{\partial\Phi_b}{\partial\mu_a})$ and $\Delta\chi$ means $(\Delta D, \Delta\mu_a)$. Of the optical-property image reconstruction algorithm, finally, the flowchart is shown as Fig. 5.

4. Results

In this research, an optical-property phantom was designed including two inclusions with a two-times contrast to background. In the x-z plane, the background dimension is 130mmx50mm and the diameters of two inclusions are 12mm and 4mm, respectively, as shown in Fig. 6. In the reconstruction, a homogeneous, lower or higher initial contrast guess for the likely area was used for comparison.

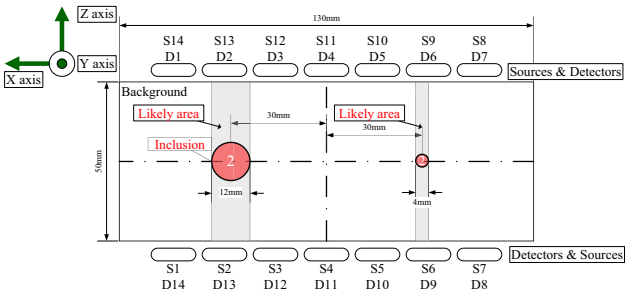

Figure 6. The cross-section diagram of the tested phantom and the likely areas used.

In this section, some results are presented. First, it is described that the advantage of the dual-direction scanning device is over that of a single-direction one by comparing with both results. Then, experimental data were used to reconstruct optical-property images.

In the dual-direction scanning, there are two mechanisms capable of be adopted as shown in Fig. 7; one is the dual-direction manner composed of two symmetric single-direction ways (S-D and D-S in red) (Fig. 7 (a)) and the other is composed of two asymmetric single-direction ways (S-D in red and *D**-*S** in brown) (Fig. 7 (b)). Figure 8 shows the results obtained from the S-D, D-S, and two-direction combination, respectively; however, it can be found that reconstructed absorption or scattering images are same as each other due to the phantom designed as being symmetric to the x-y plane. In this case, it means that half of data are redundant in spite of using a combination of two single-direction scanning. Apparently as shown in Fig. 9, the corresponding result of using the asymmetric dual-direction scanning mechanism is better than that of using a single-direction scanning or a symmetric dual-direction scanning mechanism due to the symmetry of the tested phantom being violated.

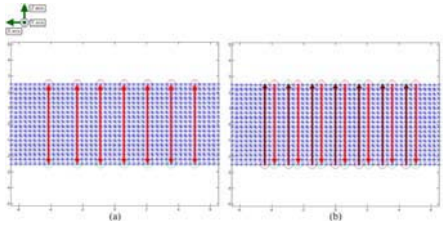

Figure 7. Dual-direction manner composed of (a) two symmetric single-direction ways (S-D and D-S) and (b) two asymmetric single-direction ways (S-D and *D**-*S**)

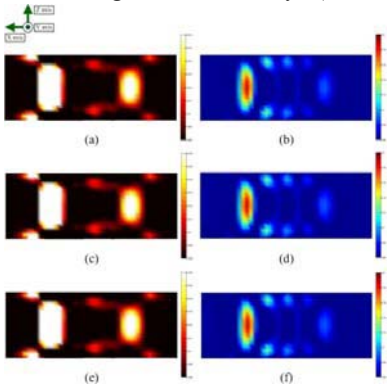

Figure 8. The results obtained from (a) the S-D, (b) D-S, and (c) a combination of two symmetric single-direction scanning, respectively.

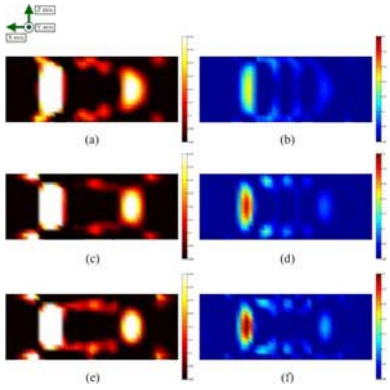

Figure 9. The results obtained from (a) the S-D, (b) D-S, and (c) a combination of two asymmetric single-direction scanning, respectively.

Reconstruction images of simulation and experiment are shown as Fig. 10 and Fig. 11, respectively, which was implemented with the combination of two symmetric single-direction scanning. In case of simulation, using a likely area of higher initial contrast could estimate the contrast and size of inclusions (Fig. 10 (e) and (f)) whereas using a likely area of the lower initial contrast may overestimate the contrast and size of inclusions (Fig. 10 (a) and (b)). However, reconstructed images using early experimental data have much more artifacts around the boundary; this related research remains ongoing.

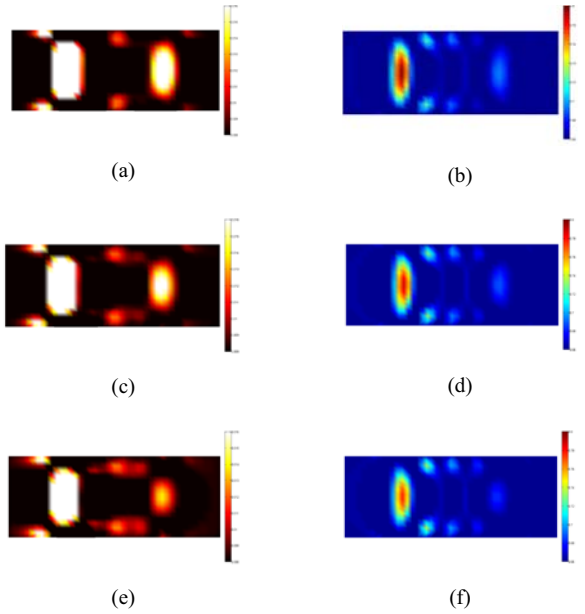

Figure 10. Absorption (left) and scattering (right) images of simulation with a (a), (b) lower initial contrast, (c), (d) homogeneous, and (e), (f) higher initial contrast.

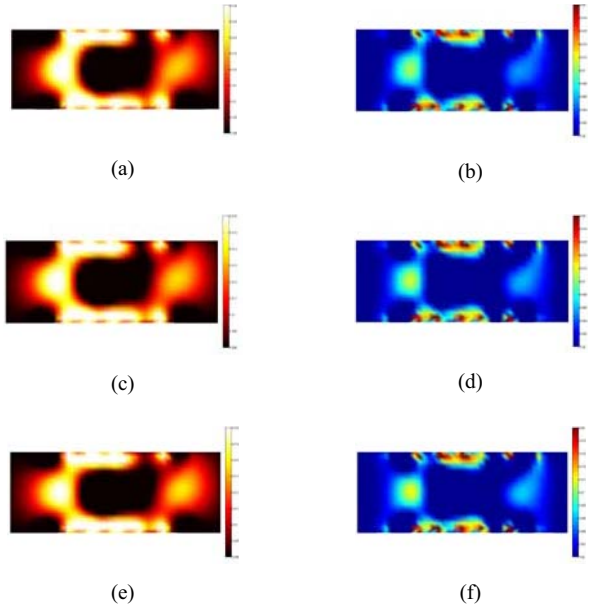

Figure 11. Absorption (left) and scattering (right) images of experiment with a (a), (b) lower initial contrast, (c), (d) homogeneous, and (e), (f) higher initial contrast

5. Concluding Remarks

Results have show that the advantage of a dual-direction scanning mechanism is able to provide a better quality of image reconstruction than a single-direction one; furthermore, this design can be much more adaptable with a pre-defined function. From the experience of our experimental work, it can be found that the reconstructed optical-property images are comparable with those achieved from the use of a likely area; much more related results will be published in near future..

References

[1] B. W. Pogue, S. P. Poplack, T. O. McBride, W. A. Wells, K. S. Osterman, U. L. Osterberg and K. D. Paulsen: "Quantitative hemoglobin tomography with diffuse near-infrared spectroscopy: Pilot results in the breast," *Radiology*, vol. 218, no. 1, pp. 261–266 , 2001.

[2] B. W. Pogue, T. O. McBride, U. L. Osterberg, and K. D. Paulsen: "Comparison of imaging geometries for diffuse optical tomography of tissue," *Optics letters*, vol. 4, no. 8, pp. 270-286, 1999.

[3] Q. Zhang, T. J. Brukilacchio, A. Li, J. J. Stott, T. Chaves, E. Hillman, T. Wu, M. Chorlton, E. Rafferty, R. H. Moore, D. B. Kopans and D. A. Boas: "Coregistered tomographic X-ray and optical breast imaging: Initial results," *Journal of Biomedical Optics*, vol. 10, no.2, pp. 024033:1-024033:9, 2005.

[4] F. E. W. Schmidt: "Development of a time-resolved optical tomography system for neonatal brain imaging," *Ph.D. thesis*, University College London, 1999.

[5] K. D. Paulsen, Ulf L. Osterberg, B. W. Pogue, and M. S. Patterson: "Optical image reconstruction using frequency-domain data: simulations and experiments," *J. Opt. Soc. Am. A*, vol.13, no.2, pp. 253-266, 1996.

[6] S. R. Arridge, M. Schweiger, M. Hiraoka and D. T. Delpy: "A finite element approach for modeling photon transport in tissue," *Med. Phys.*, vol. 20, no. 2, pp. 299-309, 1993.

[7] Q. Fang, S. A. Carp, J. Selb, G. Boverman, Q. Zhang, D. B. Kopans, R. H. Moore, E. L. Miller, D. H. Brooks and D. A. Boas: "Combined optical imaging and mammography of the healthy breast: Optical contrast derived from breast structure and compression," *IEEE Transactions on Medical Imaging*, vol. 28, no. 1, pp. 30-42 , 2009.